

# We are IntechOpen, the world's leading publisher of Open Access books Built by scientists, for scientists

5,300

Open access books available

130,000

International authors and editors

155M

Downloads

Our authors are among the

154

Countries delivered to

TOP 1%

most cited scientists

12.2%

Contributors from top 500 universities



WEB OF SCIENCE™

Selection of our books indexed in the Book Citation Index  
in Web of Science™ Core Collection (BKCI)

Interested in publishing with us?  
Contact [book.department@intechopen.com](mailto:book.department@intechopen.com)

Numbers displayed above are based on latest data collected.  
For more information visit [www.intechopen.com](http://www.intechopen.com)



# Pretargeted Theranostics

Markus Staudt, Matthias M. Herth  
and Christian B.M. Poulie

## Abstract

Personalized medicine is becoming an integral part of our healthcare system, in which theranostics play a fundamental role. Nanomedicines such as monoclonal antibodies are a commonly used targeting vector in such approaches due to their outstanding targeting abilities as well as their capabilities to function as drug delivery vehicles. However, the application of nanomedicines in a clinical setting is connected with several challenges. For example, nanomedicines typically possess slow pharmacokinetics in respect to target accumulation and excretion. For targeted radionuclide therapy, this results in high radiation burden to healthy tissue. For drug delivery systems, long circulation and excretion times of the nanomedicine complicate site-specific release approaches and limit as such the usability of these strategies. One way to circumvent these challenges is the use of pretargeting strategies, which allow to separate the accumulation and excretion of nanomedicines from the actual diagnostic or therapeutic application. As such, pretargeting allows to use theranostic concepts utilizing the same nanomedicine and determine the success chances with diagnostic measures before initiating therapy. This chapter will explain the concept of pretargeted theranostics, which pretargeting systems have thus far been developed and compare how these systems performed.

**Keywords:** radionuclide therapy, PET, SPECT, MRI, radiopharmaceuticals, bispecific antibodies, oligonucleotides, tetrazine/TCO ligation, pretargeting

## 1. Introduction

Theranostics is a portmanteau of the words therapeutics and diagnostics and is referring to a system where the *modus operandi* of both therapeutic and diagnostic aspects are combined. In this personalized medicine approach, patients are in the first phase non-invasively imaged to identify potential responders to a certain therapy (**Figure 1**) [1]. The ideal theranostic system comprises of a diagnostic and therapeutic agent, which are chemically nearly identical. In reality, the term theranostics is used in a much broader context, i.e. systems that can be used for both diagnostic and therapeutic approaches are also defined as theranostics, even if they differ in their chemical nature [2]. In this chapter, we will discuss theranostics applications mainly in the field of nuclear medicine.

Nanomedicines, especially monoclonal antibodies (mAbs), are finding an ever widespread use in theranostic radionuclide or drug delivery approaches [3]. Unfortunately, nanomedicines typically possess slow target accumulation and excretion times resulting in unwanted and often unacceptably high radiation doses to healthy tissue or limited control in drug release combined with increased

systemic toxicity [4]. Pretargeted approaches have the potential to address this challenge by separating the target accumulation process from the diagnostic or therapeutic step.

In pretargeting, a tagged nanomedicine is first administered and allowed to accumulate at its target and excrete from non-targeted tissues over the course of several hours to days. In a second step, a pretargeting agent is administered that bioorthogonally reacts with the tag of the nanomedicine, but is excreted fast from systemic circulation. As such, high and rapid accumulation at the target site can be reached while exposure of the diagnostic or therapeutic component to non-targeted tissues is minimized [5, 6]. Pretargeting is optimally suited for theranostic applications since the pretargeted vector – the nanomedicine – can initially be used for diagnostic purposes and only after having identified the feasibility of the approach, a therapeutic step is initiated (**Figure 2**). Especially in nuclear medicine, such strategy could be highly useful as within the diagnostic phase not only possible responders can be identified, but also the maximum tolerated radiation dose estimated and consequently, on an individual level, best therapeutic efficacy reached (**Figure 1**) [7].

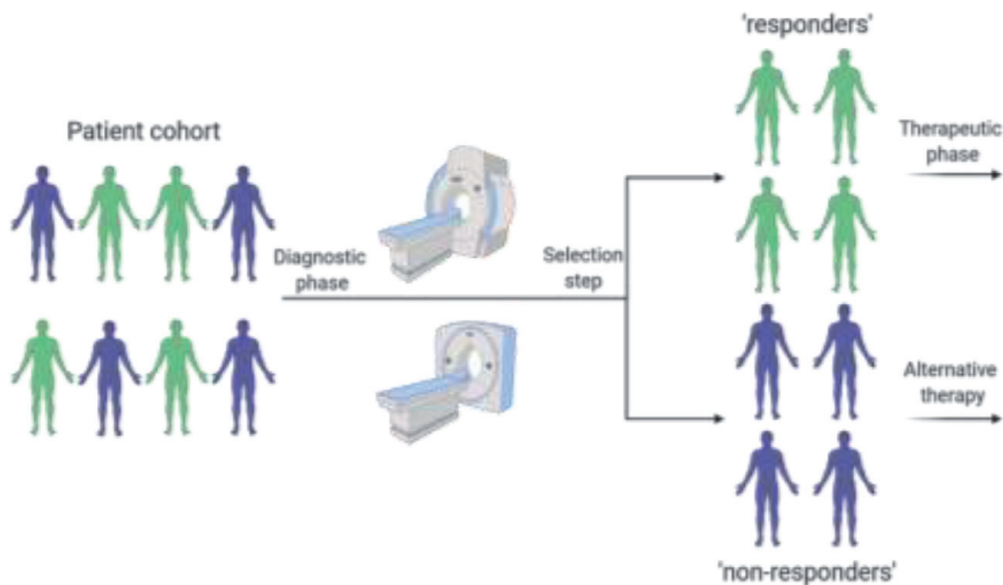


**Figure 1.** Personalized medicine. In the diagnostic phase, individuals from the patient cohort that are responding, measured as target accumulation of the nanomedicine, are separated from the non-responders. The responders can move on to the therapeutic phase, whereas for non-responders an alternative treatment form should be applied.

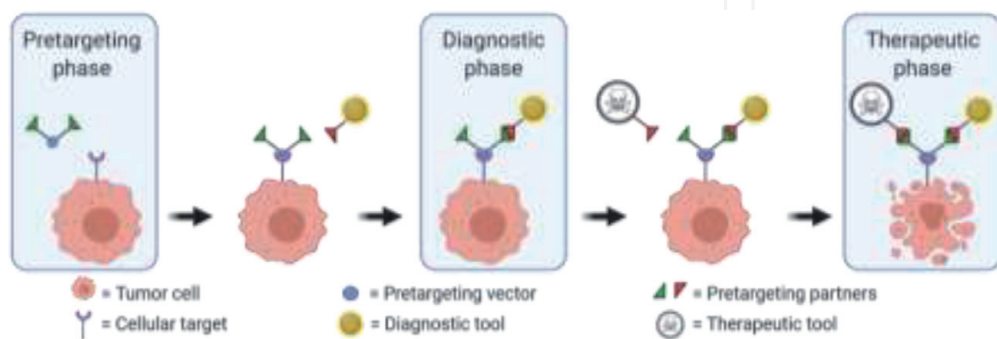


**Figure 2.** Simplified schematic overview of a typical pretargeted theranostic strategy.

## 2. Pretargeted theranostics

### 2.1 Diagnostic imaging modalities

#### 2.1.1 Positron emission tomography (PET) and single photon emission computed tomography (SPECT)

PET or SPECT are routinely used in the clinic for diagnosis or monitoring of treatment response. Their high sensitivity (the level of detection approaches tracer concentrations of  $10^{-12}$  M) combined with isotopic detection make their clinical applications unmatched [8]. Furthermore, PET can easily be applied for quantitative measurements and as such used to determine e.g. the amount of pretargeting vectors delivered to a specific target. This makes PET especially suited for personalized medicine [9]. One drawback of PET and SPECT is their limited spatial resolution, which lies within the millimeter range [10].

PET and SPECT are dependent on radionuclides that are attached to a specific ligand that is able to target e.g. a specific receptor, enzyme or protein [11]. The choice for the appropriate radionuclide depends on the context and system these diagnostic tools will be used in. For example, if diagnostic radionuclides will be attached to a nanomedicine, longer lived radionuclides are needed, as the biological half-life of the nanomedicines (accumulation or excretion) has to be matched with the physical decay half-life of the radionuclide. Typically, only after several days, nanomedicines display sufficient signal-to-background ratios for imaging purposes [4]. In case of pretargeting, radionuclides with a shorter decay half-life can be used as the good pharmacokinetic profile of small molecules results in fast accumulation and excretion [12]. This allows to use PET radionuclides such as fluorine-18, which is the most frequently used radionuclide within the clinic - due to its unique decay properties [13]. **Table 1** lists several radionuclides that can be used in PET or SPECT imaging.

#### 2.1.2 Fluorescence

While fluorophores are less harmful to tissue in comparison to the use of radionuclides, offer higher temporal and spatial resolution - up to tens of nanometers, fluorophores are majorly disadvantaged by their severely lower tissue penetration of only a few millimeters. This limitation prohibits their use for imaging of deeper lying tissues [14]. Nevertheless, due to their ease of use, fluorescence-based imaging probes are at least within preclinical development a commonly used imaging modality. A list of routinely used fluorophores and their absorption and emission maximum can be found in **Table 2**.

#### 2.1.3 Magnetic resonance imaging (MRI)

MRI is an imaging technique that does not rely on ionizing radiation and therefore has a significantly lower sensitivity (approximately  $10^{-4}$  M) compared to PET or SPECT. However, it results in better spatial resolution [15]. In the context of pretargeted theranostics, a contrasting agent is often added to the pretargeting vector - in order to enhance visibility of the target. The most commonly used contrast agent is gadolinium(III) ( $Gd^{3+}$ ), in various chelated forms and works by shortening the  $T_1$  (spin-lattice) relaxation time [16]. Another  $T_1$  signal enhancer is manganese(II)

| SPECT             |               |                | PET              |               |               |
|-------------------|---------------|----------------|------------------|---------------|---------------|
| Isotope           | $T_{1/2}$ (h) | $\gamma$ (keV) | Isotope          | $T_{1/2}$ (h) | $\beta^+$ (%) |
| $^{99m}\text{Tc}$ | 6.01          | 140            | $^{11}\text{C}$  | 0.33          | 99.8          |
| $^{111}\text{In}$ | 67.3          | 171 and 245    | $^{18}\text{F}$  | 1.83          | 96.7          |
| $^{123}\text{I}$  | 13.3          | 159            | $^{64}\text{Cu}$ | 12.7          | 17.5          |
|                   |               |                | $^{68}\text{Ga}$ | 1.13          | 89.1          |
|                   |               |                | $^{86}\text{Y}$  | 14.7          | 33.0          |
|                   |               |                | $^{89}\text{Zr}$ | 78.4          | 22.7          |
|                   |               |                | $^{124}\text{I}$ | 100.2         | 22.8          |

Their corresponding half-lives ( $T_{1/2}$ ) are noted in hours (h). For SPECT radionuclides, the energy of the gamma ( $\gamma$ ) photon is noted in keV, for PET radionuclides, their corresponding percent (%) of positron ( $\beta^+$ ) decay is noted.

**Table 1.**  
Nuclear properties of common SPECT and PET radionuclides.

| Fluorophore       | Absorption maximum [nm] | Emission maximum [nm] |
|-------------------|-------------------------|-----------------------|
| Fluorescein       | 495                     | 517                   |
| AlexaFluor 488    | 494                     | 519                   |
| Cyanine 5         | 647                     | 665                   |
| Cyanine 5.5       | 672                     | 692                   |
| Cyanine 7         | 753                     | 775                   |
| Methylene Blue    | 665                     | 684                   |
| CF-680            | 681                     | 698                   |
| IRDye-800CW       | 774                     | 789                   |
| Indocyanine Green | 776                     | 792                   |
| Dylight 800       | 777                     | 794                   |

**Table 2.**  
Absorption and emission maxima of commonly used fluorophores in PBS.

( $\text{Mn}^{2+}$ ) [17]. Several  $T_2$  (spin–spin) signal enhancers exist, but are less commonly used options. One of these are magnetic nanoparticles (MNP), such as iron oxide or iron/platinum alloys, or alternatively barium(II) ( $\text{Ba}^{2+}$ ) salts. Especially in a theranostic context, decorated MNPs are of great interest as they can simultaneously be used as passive targeting vectors - due to the enhanced permeability and retention (EPR) effect [18].

## 2.2 Therapy approaches

### 2.2.1 Radionuclide therapy

Targeted radionuclide therapy approaches have the potential to treat micrometastases and residual tumor tissue remaining after surgical resection – both of which play a major role in the mortality of cancer patients. Currently, only very few radionuclide therapies have found application in clinical practice [19]. This is likely to change in the coming decade, as radionuclide therapy may be more effective than standard therapeutic strategies, e.g. external radiation therapy or state-of-the-art chemotherapy. Two types of radiation can be used in radionuclide-based therapies, namely  $\alpha$ - and

| Isotope           | $T_{1/2}$ (h) | Decay                  | Photon energy (keV) | %    |
|-------------------|---------------|------------------------|---------------------|------|
| $^{67}\text{Cu}$  | 61.8          | $\beta^-$              | 185                 | 49   |
| $^{90}\text{Y}$   | 64.6          | $\beta^-$              | 1700                | 0.01 |
| $^{131}\text{I}$  | 192.5         | $\beta^-$              | 364                 | 81   |
| $^{177}\text{Lu}$ | 159.5         | $\beta^-$              | 208                 | 11   |
| $^{188}\text{Re}$ | 17.0          | $\beta^-$              | 155                 | 15   |
| $^{211}\text{At}$ | 7.2           | $\alpha$               | 79                  | 21.3 |
| $^{213}\text{Bi}$ | 0.8           | $\alpha$               | 440                 | 26   |
| $^{212}\text{Pb}$ | 10.6          | $\beta^-$ and $\alpha$ | a                   | a    |
| $^{225}\text{Ac}$ | 238.1         | $\beta^-$ and $\alpha$ | a                   | a    |

Their corresponding half-lives ( $T_{1/2}$ ) are noted in hours, the energy of the photon is noted in keV.  
 a. Multiple photons, at different energies, are emitted, due to multiple daughter radionuclides.

**Table 3.**  
 Nuclear properties of common therapeutic radionuclides.

$\beta^-$ -radiation. In general,  $\alpha$ -emitting radionuclides are far more effective due to the significantly higher linear energy transfer (LET) (approx. 100 keV/ $\mu\text{m}$ ), compared to the much lower LET of  $\beta^-$ -emitting radionuclides (approx. 0.2 keV/mm) [4]. However,  $\alpha$ -emitters might even be too toxic for many applications.

Just like for the diagnostic case, the choice of radionuclide is highly dependent on the context and system, these radionuclides are used in. With the exception of iodine-131 and astatine-211, all other commonly used radionuclide are radiometals and need to be chelated. As such, these radiopharmaceuticals are typically very polar (**Table 3**). Another factor to be considered is the limited availability of certain radionuclides, such as astatine-211, bismuth-213, lead-212 or actinium-225 [20]. Additionally, lead-212 and actinium-225 have several radioactive daughter nuclides which contribute to radiotoxicity throughout the body when released from the chelator and distributed throughout the body. Due to the high energy released after the first decay event, typically daughter nuclides are released from the chelator and not bound to the chelator any longer [21].

### 2.2.2 Chemotherapy

Chemotherapy involves the use of highly cytotoxic compounds which are supposed to kill cancer cells more efficiently than healthy cells. In the context of pretargeted approaches, these compounds work in exactly the same manner as in standard chemotherapy approaches, with the crucial difference that they are delivered from the nanomedicine to the target side and then (selectively) released e.g. using click-to-release strategies [22, 23]. A locally increased concentration of the chemotherapeutic is as such achievable, whereas the systemic concentration and its subsequent toxicity is reduced [24]. A few examples of cytotoxic compounds that have been used in conjunction with pretargeted theranostics are paclitaxel, mertansine or doxorubicin [25–27]. However, in theory any cytotoxic drug could be used.

## 2.3 Pretargeting strategies and their applications as potential Theranostics

### 2.3.1 Biotin/streptavidin binding

Pretargeting approaches based on the strong, non-covalent interaction between biotin and streptavidin, with a  $K_d$  in the order of approximately  $10^{-14}$  M were

among the earliest strategies to be successfully applied for pretargeted radioimmuno-imaging and –therapy [4]. In fact, several clinical studies were initiated and are ongoing [28–30]. The strong binding affinity is leveraged by most commonly attaching the tetrameric streptavidin - capable of binding up to four biotins - to a mAb and after sufficient accumulation of this pretargeting vector, radiolabeled biotin is injected as the targeting agent. Despite these successes, reports of this strategy in a theranostic setting are limited. This might be due to the observed increased levels of human anti-streptavidin antibodies, potentially leading to allergic reactions upon subsequent applications [31, 32].

### 2.3.2 Bispecific antibodies

Bispecific antibodies (bsAb) are artificially constructed immunoconjugates, possessing both an antigen-binding fragment (Fab) - typically targeting an over-expressed receptor on the target cell surface - and an anti-hapten Fab. This allows for targeting the cancer cell while also retaining high affinity to a hapten of choice, which can be used to bind imaging or therapeutic vectors after sufficient accumulation time of the bsAb. Antibody fragments are typically derived from the immunoglobulin G (IgG) antibody, which consists of two Fab sites and a constant fragment crystallizable (Fc) region. Digestion of IgG by pepsin yields the  $F(ab')_2$  fragment, which can be further split into two Fab' fragments by mild reduction. Digestion by papain on the other hand yields two Fab fragments. Removal of the two remaining constant domains and relinking them yields fusion proteins called single-chain variable fragment (scFv) (**Figure 3**) [33].

Aniline modified DOTA (DOTA-Bn, **Figure 4**) can act as an efficient chelator for a large variety of (radio)metals and also serve as the hapten. Haptens are small molecular entities that are used to engineer antibodies possessing high affinity to these small molecules, allowing for fragmentation into smaller hapten-binding scFv. In the case of DOTA-Bn, the scFv C825 is capable of binding DOTA-Bn chelated yttrium ( $Y^{3+}$ ) and lutetium ( $Lu^{3+}$ ) with picomolar affinity ( $\sim 15$  and  $11$  pM respectively). This allowed for construction of a IgG-scFv bsAb huA33-C825 (**Figure 4**) targeting GPA33-positive human colorectal cancer cell lines SW1222 [34]. Utilizing this system, SW1222 xenograft bearing mice were subjected to three treatment cycles of pretargeted immunotherapy (PRIT) consisting of injection of bsAb injection, followed by injection of a dextran-hapten clearing agent 24 hours later and injection of  $[^{177}Lu]Lu$ -DOTA-Bn after four more hours. SPECT/CT was utilized to follow the treatment, showing high specific tumor uptake ( $\sim 7\%$  ID/g) and only low uptake (10–15 fold lower) in the liver, the spleen and the kidneys. After three cycles of treatment with 55.5 MBq activity of  $[^{177}Lu]Lu$ -DOTA-Bn (at days 7, 14 and 21 after tumor inoculation), 100% histologic cures in 9 of 9 treated

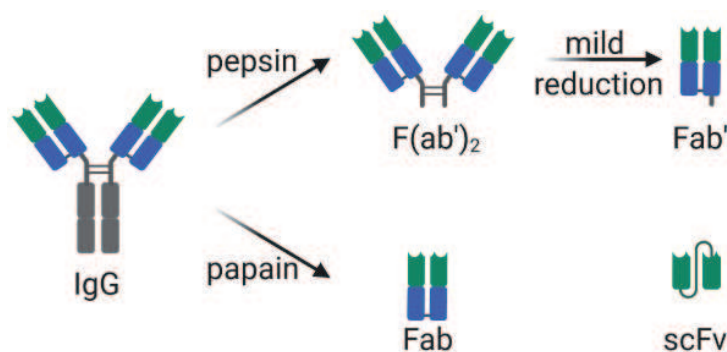


**Figure 3.** IgG antibody and its fragments used in the construction of bispecific antibodies.

animals were achieved. Therefore, this approach allows for a theranostic platform with a single radiopharmaceutical entity, allowing for SPECT imaging and providing tumor radiation estimate by changing the amount of radioactivity administered. However, using a therapeutic radionuclide for clinical diagnosis is not optimal since only low amounts can be administered, which often result in insufficient count rates for imaging purposes.

In a similar approach, the food and drug administration (FDA)-approved anti-HER2 antibody trastuzumab, modified with scFv C825 (**Figure 4**), was utilized to target HER2-positive human breast cancer BT-474 xenograft bearing mice [35]. Although internalizing targets like HER2 are normally not suitable for PRIT, it was found that 24 hours post injection of the bsAb around 11% of the initially bound trastuzumab-C825 remained on the cell surface. Using a clearing agent 24 hours after injection of the bsAb, followed by 5.6 MBq of [ $^{177}\text{Lu}$ ]Lu-DOTA-Bn allowed for biodistribution-based dosimetry, showing ~7% ID/g uptake in the tumor with high tumor to blood and kidney ratios (T/B: ~27, T/K: ~10). Given this, the estimated maximum tolerated activity was calculated to be 180 MBq, with blood being the dose-limiting organ. In following therapeutic studies, a single-cycle treatment with 55.5 MBq of [ $^{177}\text{Lu}$ ]Lu-DOTA-Bn was found to lead to 100% complete response (CR) in small tumors up to 30 mm<sup>3</sup>, but did not produce a high CR in medium sized tumors (100–400 mm<sup>3</sup>). The latter could be successfully treated through three cycle PRIT using 55.5 MBq of [ $^{177}\text{Lu}$ ]Lu-DOTA-Bn, showing 25% complete tumor disappearance and 75% regression to palpitation threshold. Once again, SPECT/CT was used to monitor treatment progression 24 hours p.i. of 55.5 MBq of [ $^{177}\text{Lu}$ ]Lu-DOTA-Bn.

In clinical practice, PET results in better spatial resolution than SPECT. In this regard, a PET tracer based hapten probe was developed [36]. Hapten [ $^{86}\text{Y}$ ]Y-DOTA-Bn was synthesized and used to image a bsAb targeting GPA33-positive cancers [37]. The biodistribution data was in line with the one determined using [ $^{177}\text{Lu}$ ]Lu-DOTA-Bn. Consequently, hapten [ $^{86}\text{Y}$ ]Y-DOTA-Bn can be used as a

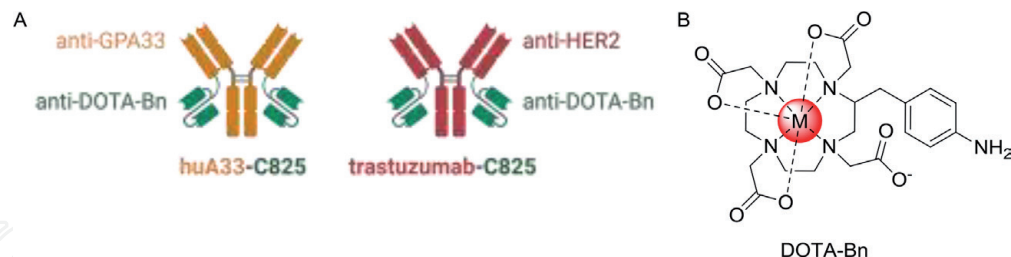


**Figure 4.**  
A: Schematic representation of bsAb huA33–825 and trastuzumab-C825. B: Structure of DOTA-Bn chelating  $\text{M}^{3+}$ .

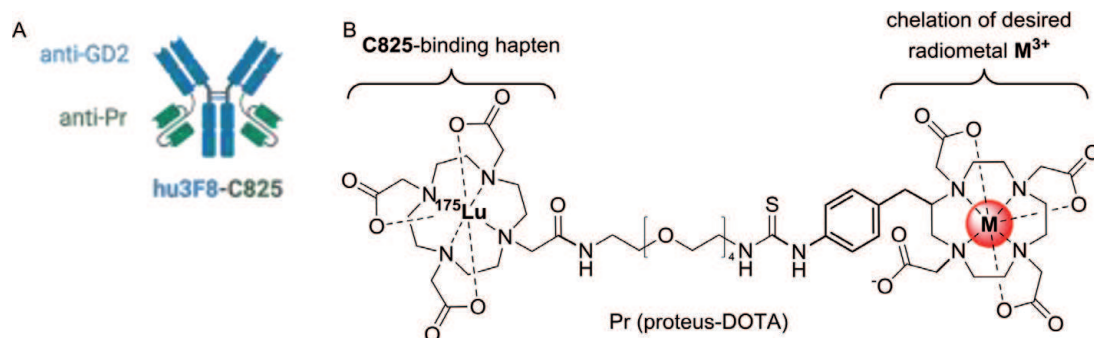


**Figure 5.**  
A: Schematic representation of bsAb hu3F8–C825. B: Structure of proteus-DOTA (Pr) chelating non-radioactive  $^{175}\text{Lu}^{3+}$  and the radiometal of choice  $\text{M}^{3+}$ .

surrogate for the  $^{177}\text{Lu}$ -labeled derivative. Better diagnostic value and reduced radiation dose should be possible for clinical applications using  $^{86}\text{Y}$ -DOTA-Bn.

While the hapten DOTA-Bn allows for straight forward incorporation of yttrium and lutetium, it comes with severe limitations to the modularity of the system as the affinity of the hapten towards scFv C825 varies depending on the chelated metal. This effect was observed in a study on the anti-DOTA antibody scFv –hu3F8-C825 (**Figure 5**), which bound  $^{177}\text{Lu}$ -DOTA-Bn with picomolar affinity, whereas  $^{225}\text{Ac}$ -DOTA-Bn was found to have severely decreased binding [38]. This resulted in a decreased tumor accumulation. To circumvent this problem, a novel construct bearing two DOTA-moieties called proteus-DOTA (Pr, **Figure 5**) was synthesized. By chelating non-radioactive, isotopologic lutetium-175 in one of the DOTA moieties, the construct is able to bind with high affinity to previously utilized scFv C825, while retaining the ability to chelate a radiometal of choice in the second DOTA chelator (**Figure 5**). Using this system, high tumor and relatively low normal tissue accumulation of both  $^{111}\text{In}$ -Pr and  $^{225}\text{Ac}$ -Pr was achieved. This approach was then successfully employed in a pretargeted therapeutic approach in treating three solid human cancer xenograft models of colorectal cancer (GPA33), breast cancer (HER2), and neuroblastoma (GD2) using the respective anti-tumor/C825 bsAb, followed by injection of a dextran clearing agent after 24 h and four hours later the radiohapten  $^{225}\text{Ac}$ -Pr.

Another promising approach lies in changing the utilized hapten to the small peptidic sequence histamine-succinyl-glycine (HSG). In this respect, the bivalent hapten IMP288 modified with two HSG and DOTA and the trivalent bsAb TF2 were identified to be the most promising pair for clinical translation of this pretargeted system (**Figure 6**) [39]. The trivalent bsAb TF2 was build up through a dock-and-lock approach, linking two anti-carcinoembryonic antigen (CEA) Fabs, binding to the cancers expressing CEA, and one anti-HSG Fab linked through two disulfide bounds (**Figure 6**). This approach allows to label IMP288 with a set of radiometals for both therapeutic and diagnostic purposes. Subsequent preclinical studies in mice bearing CEA-expressing colonic tumors showed very low uptake in normal tissues - apart from the kidneys (~2% ID/g) – and high tumor uptake using PET or SPECT imaging with  $^{68}\text{Ga}$ -Ga-IMP288 (~11% ID/G) or  $^{111}\text{In}$ -In-IMP288 (~26% ID/G) [40]. These imaging data was successfully used for dose estimations of  $^{177}\text{Lu}$ -Lu-IMP288 and  $^{213}\text{Bi}$ -Bi-IMP288 [41, 42].

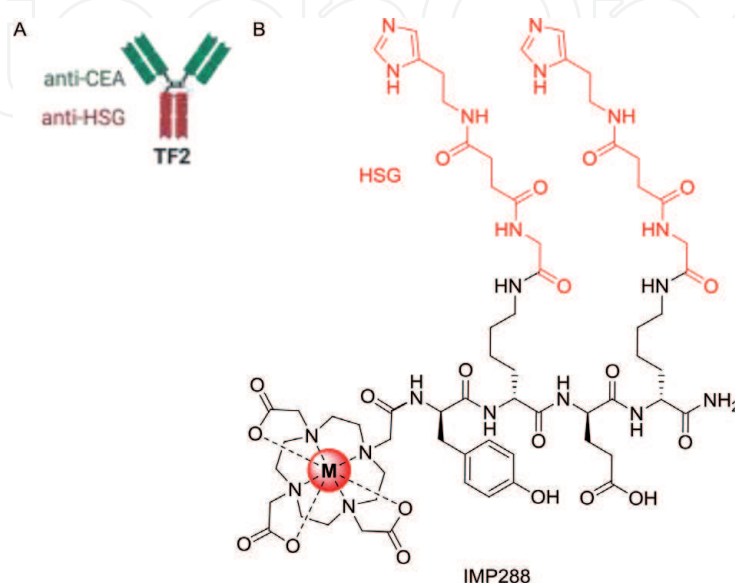


**Figure 6.**

A: Schematic representation of bsAb TF2. B: Structure of IMP288 chelating  $\text{M}^{3+}$ .

Given this promising data, the IMP288/TF2 system was translated into the clinic using [ $^{111}\text{In}$ ]In-IMP288 in the imaging cycle for predictive patient-specific dosimetry and [ $^{177}\text{Lu}$ ]Lu-IMP288 as the therapeutic agent. Herein, it was shown, that the treatment of metastatic colorectal cancer patients at activity doses ranging from 2.5 to 7.4 GBq of [ $^{177}\text{Lu}$ ]Lu-IMP288 was safe, but only one of the four planned treatment cycles was carried out since all patients showed progression of the disease, 8 weeks after the first cycle [43]. Also immunogenic responses towards the humanized bsAb TF2 were observed in 11 out of 21 patients. Surprisingly, this immunogenic response was only observed to a very limited degree in one out of eight patients in another study using the same system on advanced lung cancer patients [44].

### 2.3.3 Oligonucleotides

A more recently employed pretargeting strategy relies on the strong interaction between complementary strands of oligonucleotides. Although unmodified desoxy-ribonucleic acids (DNAs, **Figure 7**) and ribonucleic acids (RNAs, **Figure 7**) are not suitable for in vivo use due to their rapid degradation by nucleases, recent developments of peptide nucleic acids (PNAs, **Figure 7**) have shown promise in pretargeting. PNAs increase enzymatic stability by replacing the sugar-phosphate backbone of DNAs/RNAs by a pseudo-polypeptidic backbone consisting of a *N*-(2-aminoethyl)-glycine units [45]. PNAs retain Watson-Crick base-pair binding to complementary PNA, DNA or RNA strands. The interaction between PNA/PNA is with greater specificity and binding affinity compared to the corresponding DNA/DNA analogs. A fourth alternative to DNAs, which is stable to enzymatic degradation are phosphorodiamidate morpholino oligomer (morpholinos, **Figure 7**) [46]. Here, the sugar-phosphate moiety is replaced by a methylenemorpholine ring, linked through phosphordiamidate groups.

In a pretargeted study using the PNA-affibody conjugated with  $Z_{\text{HER2.342}}\text{-SR-HP1}$  and a complementary PNA-based DOTA derivative (HP2), the biodistribution patterns of [ $^{68}\text{Ga}$ ]Ga-HP2 and the therapeutic PNA [ $^{177}\text{Lu}$ ]Lu-HP2 were evaluated in SKOV3 xenografts [47]. Overall, quite profound differences in biodistribution between [ $^{68}\text{Ga}$ ]Ga-HP2 (~6% ID/g tumor and ~9% kidney accumulation) and [ $^{177}\text{Lu}$ ]Lu-HP2 (~12% ID/g tumor and ~8% kidney accumulation) were found, making precise prediction of therapeutic uptake of the latter difficult [48]. This study exemplified that the choice of a theranostic pair, here gallium-68 and lutetium-177, can have an influence on the biodistribution of the labeled radiopharmaceutical. Different stability or altered dipole moments within the chelated structure are some of the possible reasons for this behavior.

### 2.3.4 Tetrazine/*trans*-cyclooctene (TCO) ligation

Another strategy for pretargeting involves the covalent bond forming ligation between an 1,2,4,5-tetrazine and a TCO [49]. The reaction is initiated with an enthalpically driven strain release of the inverse electron demand Diels-Alder

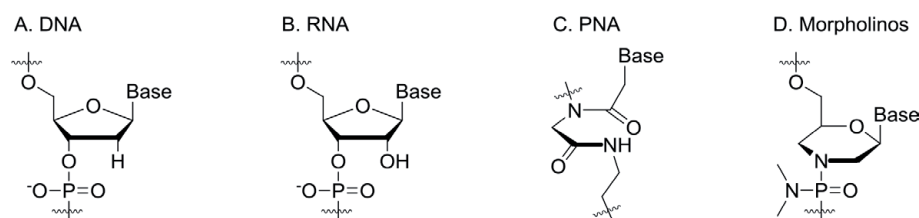


**Figure 7.**  
Structure of DNA, RNA, PNA and morpholino oligonucleotides.

(IEDDA) cycloaddition. The cycloaddition is followed by an entropically driven retro Diels-Alder reaction, in which molecular nitrogen is expelled, making this reaction irreversible (**Figure 8A**) [50]. Various substituted tetrazines and TCO analogues can be used for this ligation, all differing in their corresponding speed kinetics and in vivo stability. As a general trend, with increasing in vivo stability, a decrease in speed kinetics is observed and vice versa.

The most common approach for pretargeting using the tetrazine ligation is based on TCO-modifications of nanomedicines, which act as pretargeting vectors [51]. These vectors can first be imaged by a tetrazine probe and followed up with a treatment phase, using a therapeutic, tetrazine based probe. For example, the CEA targeting mAb 35A7 was decorated with approximately 3–4 TCO tags and four different [ $^{177}\text{Lu}$ ]-bispyridyl-tetrazine probes used to evaluate the effectiveness of the pretargeted approach. SPECT was used to determine the in vivo biodistribution of the various tracers and gain insights about maximum tolerated dose. The most promising probe was used in a treatment approach and a projected dose of 40 MBq was applied. This resulted in a significant slow-down of tumor progression, for up to 13 days, after which the tumors started to grow again, albeit much slower as compared to the control group [52].

In a similar approach, using a human colorectal carcinoma mouse model, a transmembrane glycoprotein (the A33 antigen) targeting mAb huA33 was decorated with approximately 2–3 TCO tags. Two different tetrazine probes were administered [53]. 24 hours after administration of the huA33-TCO a [ $^{64}\text{Cu}$ ]-H-tetrazine probe was injected and used for diagnostic PET imaging. This was followed by an injection of a [ $^{177}\text{Lu}$ ]-H-tetrazine probe, after an additional 24 hours (48 hours post mAb injection). It was estimated that after the injection of the diagnostic tetrazine, roughly 64% of the TCOs on the mAb were available, for the therapeutic tetrazine probe. This study showed that the same targeting vector can be used for imaging and therapy purposes and as such for real theranostic approaches. The same group also evaluated a  $^{67}\text{Cu}$ -labeled H-tetrazine in the same setup for  $\beta^-$  radiotherapy [54]. Within this study, the authors compared the therapeutic effect of pretargeted radioimmunotherapy (PRIT) to conventional radioimmunotherapy (RIT). Even though RIT achieved a comparable survival rate, at lower injected dose, compared to PRIT, it is important to note that PRIT significantly reduced the individual organ dose rates, in comparison to RIT, i.e. the radiation dose to the blood for the PRIT strategy

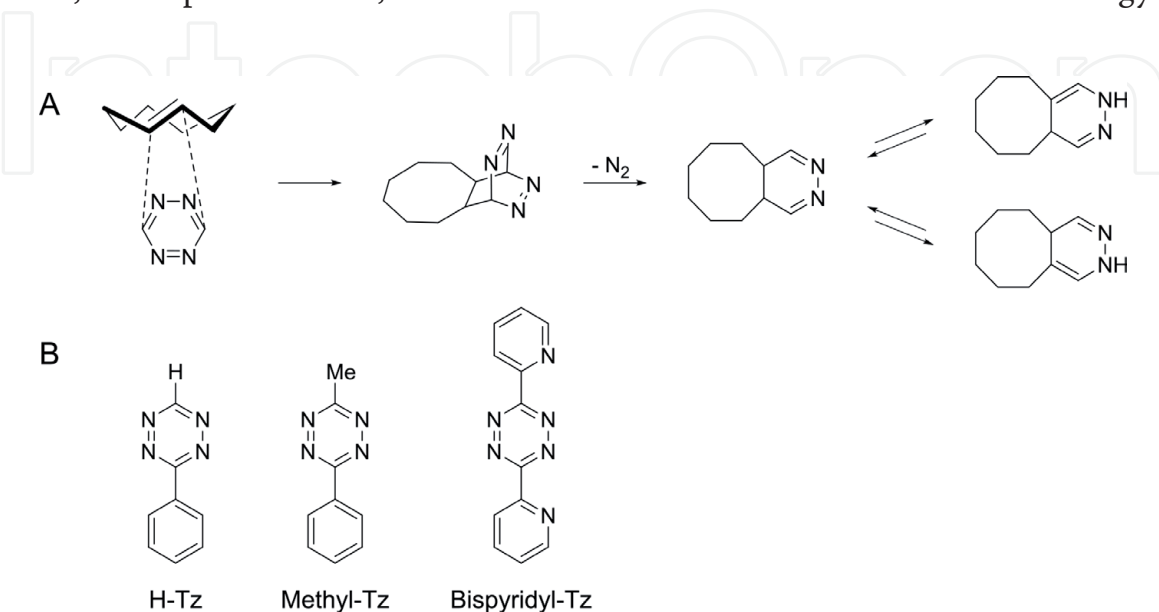


**Figure 8.** (A) Mechanism of the tetrazine/TCO ligation. (B) Chemical scaffold of a H-, a methyl- and a bispyridyl-tetrazine.

was 5.9 cGy/MBq, compared to 71.3 cGy/MBq for the RIT strategy, highlighting the main advantage of PRIT over RIT. The authors argued that the PRIT strategy can be further optimized in regards of timing of the dosing regimen, in order to achieve optimal dose rates to the tumor.

In addition to small molecule tetrazine derivatives, also tetrazine functionalized nanocarriers, such as human serum albumin (ALB), can be used as pretargeting vectors. These structures can additionally be modified e.g. with chemotherapeutic agents or fluorophores. Such a strategy was used for trastuzumab, a human epidermal growth factor receptor 2 positive (HER2+) targeting mAb. This mAb was decorated with six TCO moieties and two CF-680 near infrared (NIR) fluorophores [55]. After eight hours, a ALB nanocarrier was injected containing approximately 2–3 paclitaxel molecules, 15 methyl-tetrazines and two DyLight 800 (DL-800) NIR fluorophores. Imaging studies revealed that the tumor uptake was twice as high in mice after two days in the pretargeted group compared to the control group. Also, treated animals only showed a relative increase of tumor volume of 3%, whereas the control group saw an increase of 14%. In another study, eight TCO's were attached to 5D3, a prostate-specific membrane antigen (PSMA) targeting mAb, as well as eight TCO to its F(ab')<sub>2</sub> fragments [56]. Both moieties were additionally decorated with two AlexaFluor 488 (AF-488) fluorophores. ALB was used as the pretargeting agent and possessed 10 methyl-tetrazine handles, two rhodamine fluorophores and approximately 3–4 mertansine molecules, as a therapeutic component. Imaging studies revealed, that the F(ab')<sub>2</sub> fragments internalized faster compared to the whole mAb. Faster internalization is, however, disadvantageous since the internalized targeting vector is not available for the ligation with ALB. This nanocarrier cannot cross the cell membrane. Consequently, less cytotoxic drug can reach its target. No in vivo evaluation of this approach was performed.

Recently, a new click-to-release strategy was described which results in local increased drug concentration and as such increased treatment efficacy. In such an approach, the TCO component acts as a bioorthogonally click partner as well as a drug releasing component. The initial click mechanism is also based on the IEDDA (Figure 8A). However, the formed 4,5-dihydropyridazine will partly tautomerize to 1,4-dihydropyridazine which can lead to a release - via a self-immolative cascade reaction - of the chemotherapeutic drug in allylic position (attached e.g. via a carbamate to the TCO) (Figure 9). Such a TCO is also called release TCO (rTCO). This click-to-release strategy has also been employed in a theranostic context. For example, in tumor bearing mice expressing the tumor-associated glycoprotein-72 (TAG72), a CC49 diabody – targeting this glycoprotein and side-specifically conjugated to a rTCO decorated with monomethyl auristatin E (MMAE) – was evaluated [57]. Mice were injected with the diabody 48 prior to injection of an

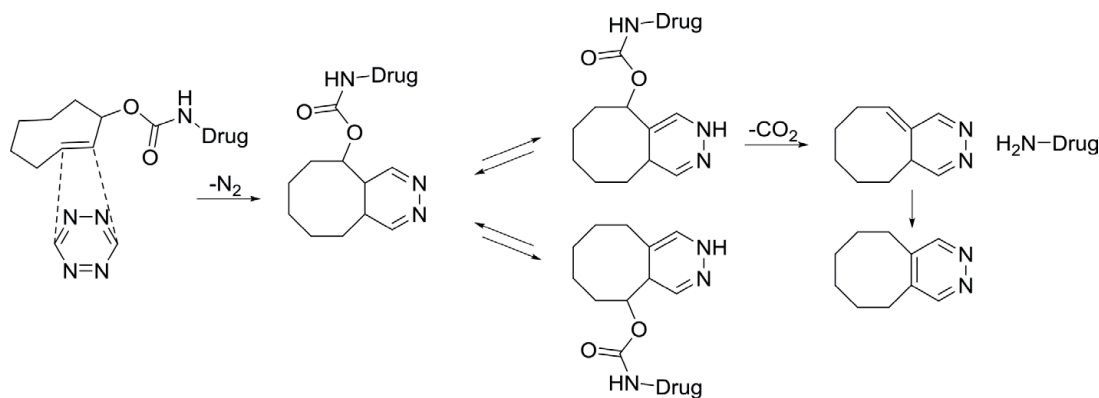


**Figure 9.**  
*Mechanism of the click-to-release reaction.*

$^{111}\text{In}$ -labeled releaser bisalkyl-tetrazine. This set-up allowed to image the release via SPECT. In a different setup, [ $^{111}\text{In}$ ]bispyridyl-tetrazine was used to determine the diabody tumor uptake, as bispyridyl-tetrazines have extremely poor release capabilities for the used rTCO. The gained information was then used to design a treatment study. Four cycles, over a period of two weeks, were used in this study and extended the median survival by 34–39 days. In a different study, a PEGylated hyper-branched polymeric (HBP) nanocarrier was developed bearing rTCOs bound to the drug doxorubicin [58]. In order to achieve a modular approach, HBP was bound to a bsAb, which could selectively interact with PEGs of the HBP with one binding site, whereas the other binding site simultaneously target with the epidermal growth factor receptor (EGFR) or TAG72. A  $^{64}\text{Cu}$ -labeled H-tetrazine was used both as the releaser and as an imaging component. This theranostic approach was evaluated in mice bearing MCF7 and MDA-MB-468 tumors. Highest release of doxorubicin was found when the tetrazine was injected 24 hours post nanocarrier injection. Furthermore, better release was observed in non-internalizing targets compared to internalizing targets, as the polar tetrazine was not able to cross the cell membrane.

Lastly, dextran-coated iron oxide MNPs (~25 nm in size) were surface modified with methyl-tetrazines and the NIR fluorophore cyanine5.5 (Cy5.5) [59]. The MNP uptake was monitored by fluorescence, as well as by  $T_2$ -weighted MRI. Targeting of these MNP was based on the EPR effect. Conceptually, selective drug release should be induced by a small molecule drug-TCO conjugate which should find the MNP-tetrazine modified targeting vector in vivo and upon reaction release the drug load. Unfortunately, the release was only in vitro, in MDA-MB-231 cells. As such, no real conclusion about the in vivo efficacy can be drawn as well as of the theranostic abilities of the system.

### 2.3.5 Strain-promoted azide-alkyne cycloaddition (SPAAC)

SPAAC has been applied in pretargeting. The reaction is based on a [3 + 2] cycloaddition between an azide and a strained alkyne (**Figure 10**). Opposed to the copper-catalyzed azide-alkyne cycloaddition (CuAAC), this reaction is metal free and instead entirely entropy driven. Various different constrained alkynes can be used for this biorthogonal reaction, i.e. difluorocyclooctynes (DIFO), bicyclononyne (BCN), dibenzocyclooctynes (DIBO), biarylazacyclooctynone (BARAC), among others. However, the most used alkyne is azadibenzylcyclooctyne (ADIBO/DIBAC), commonly referred to as DBCO. However, the feasibility of the SPAAC appears to be very limited due to its very slow reaction kinetics [60].

### 2.3.6 Miscellaneous

Besides the previously mentioned strategies, some lesser known and underexplored strategies exist. These are all based on high affinity interactions. One such set of interaction partners is based on the high affinity ( $\sim 5 \times 10^4 \text{ M}^{-1}$ ) between

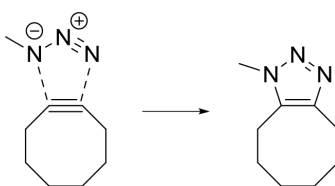


**Figure 10.** Mechanism of the strain-promoted azide-alkyne cycloaddition (SPAAC).

| <i>Pretargeting system</i> | <i>Rate constants [M<sup>-1</sup> s<sup>-1</sup>]</i> | <i>In vivo stability</i> | <i>Clinical studies</i> | <i>Benefits and limitations</i>   |
|----------------------------|---|--------------------------|-------------------------|---|
| bsAb                       | 10 <sup>3-5</sup>                                     | High                     | Yes                     | + Highly specific binding to variety of cellular targets<br>+ Straight forward accessibility through dock-and-lock approach<br>- Reversible binding between hapten and bsAb<br>- Lower tumor uptake compared to other methods |
| PNA                        | 10 <sup>5</sup>                                       | High                     | No                      | + Stable to enzymatic degradation<br>+ Potentially allows for administering two different complementary strands<br>- Increased complexity to incorporate clearing agents<br>- Challenging preparation                         |
| SPAAC                      | 10 <sup>-1-10<sup>-2</sup></sup>                      | Low                      | No                      | + Easy access to pretargeting pairs<br>- Low reactivity requires high molar ratios between pretargeting pairs   |
| TCO-Tz ligation            | 10 <sup>3-6</sup>                                     | Moderate                 | No                      | + Excellent speed kinetics<br>- Tetrazine synthesis challenging   |

**Table 4.**  
 Comparison of the pretargeting strategies utilized in pretargeted theranostics [4].

β-cyclodextrin, as the host and an adamantane derivative as the guest molecule [61]. This approach has been used in hepatic radioembolization where a macro ALB aggregate (MAA) was decorated with approximately 10<sup>8</sup> adamantane derivatives and used as the pretargeting vector. Poly(isobutyl methacrylate) (PIMBA) functionalized with 10 β-cyclodextrin handles was used as the pretargeting agent [62].

### 2.3.7 Comparison of the pretargeting strategies

## 3. Conclusion

The recently seen rapid increase in development of novel pretargeted conjugation strategies allowed for pretargeted PET imaging and α/β<sup>-</sup> therapy resulting in lower off-target toxicity and overall radiation doses. Despite preclinical successes, the increased complexity of the pretargeting approach still hampers further clinical translation, resulting in only few pretargeted theranostics being clinically investigated. Since the required multicomponent approach comes with high entry barriers of current good manufacturing practice (cGMP) production, the pretargeting approach must result in undoubtful benefits over more traditional imaging or treatment options. Although theranostics come with the large benefit of combining imaging and therapeutic agents, allowing for optimized treatment parameters, still more clinical trials need to be initiated and deliver prove of increased efficacy and decreased off-target toxicity to justify the inherently increased treatment challenges.

## Acknowledgements

C.B.M.P acknowledges funding by the BRIDGE – Translational Excellence Programme at the Faculty of Health and Medical Sciences, University of Copenhagen, funded by the Novo Nordisk Foundation (grant agreement no.

NNF18SA0034956). Further, this project has received funding from the European Union's EU Framework Programme for Research and Innovation Horizon 2020, under grant agreement no. 668532.

### **Conflict of interest**

The authors declare no competing financial interest.

IntechOpen

### **Author details**

Markus Staudt<sup>1</sup>, Matthias M. Herth<sup>1,2\*</sup> and Christian B.M. Poulie<sup>1\*</sup>

<sup>1</sup> Department of Drug Design and Pharmacology, University of Copenhagen, Copenhagen, Denmark

<sup>2</sup> Department of Clinical Physiology, Nuclear Medicine and PET, Rigshospitalet, University Hospital, Copenhagen, Denmark

\*Address all correspondence to: [matthias.herth@sund.ku.dk](mailto:matthias.herth@sund.ku.dk) and [christian.poulie@sund.ku.dk](mailto:christian.poulie@sund.ku.dk)

### **IntechOpen**

© 2021 The Author(s). Licensee IntechOpen. This chapter is distributed under the terms of the Creative Commons Attribution License (<http://creativecommons.org/licenses/by/3.0>), which permits unrestricted use, distribution, and reproduction in any medium, provided the original work is properly cited. 

## References

- [1] S. Jeelani, R. Jagat Reddy, T. Maheswaran, G. Asokan, A. Dany, and B. Anand, "Theranostics: A treasured tailor for tomorrow," *J. Pharm. Bioallied Sci.*, vol. 6, no. 5, p. 6, 2014, doi: 10.4103/0975-7406.137249.
- [2] S. Shrivastava, S. Jain, D. Kumar, S. L. Soni, and M. Sharma, "A Review on Theranostics: An Approach to Targeted Diagnosis and Therapy," *Asian J. Pharm. Res. Dev.*, vol. 7, no. 2, pp. 63-69, Apr. 2019, doi: 10.22270/ajprd.v7i2.463.
- [3] E. J. L. Stéen *et al.*, "Pretargeting in nuclear imaging and radionuclide therapy: Improving efficacy of theranostics and nanomedicines," *Biomaterials*, vol. 179, pp. 209-245, Oct. 2018, doi: 10.1016/j.biomaterials.2018.06.021.
- [4] E. J. L. Stéen *et al.*, "Pretargeting in nuclear imaging and radionuclide therapy: Improving efficacy of theranostics and nanomedicines," *Biomaterials*, vol. 179, pp. 209-245, Oct. 2018, doi: 10.1016/j.biomaterials.2018.06.021.
- [5] S. Hapuarachchige and D. Artemov, "Theranostic Pretargeting Drug Delivery and Imaging Platforms in Cancer Precision Medicine," *Front. Oncol.*, vol. 10, Jul. 2020, doi: 10.3389/fonc.2020.01131.
- [6] F. C. J. van de Watering, M. Rijpkema, M. Robillard, W. J. G. Oyen, and O. C. Boerman, "Pretargeted Imaging and Radioimmunotherapy of Cancer Using Antibodies and Bioorthogonal Chemistry," *Front. Med.*, vol. 1, Nov. 2014, doi: 10.3389/fmed.2014.00044.
- [7] U. Eberlein, M. Cremonesi, and M. Lassmann, "Individualized Dosimetry for Theranostics: Necessary, Nice to Have, or Counterproductive?," *J. Nucl. Med.*, vol. 58, no. Supplement 2, pp. 97S-103S, Sep. 2017, doi: 10.2967/jnumed.116.186841.
- [8] T. F. Massoud, "Molecular imaging in living subjects: seeing fundamental biological processes in a new light," *Genes Dev.*, vol. 17, no. 5, pp. 545-580, Mar. 2003, doi: 10.1101/gad.1047403.
- [9] O. Arrieta, L.-A. Medina, E. Estrada-Lobato, L.-A. Ramírez-Tirado, V.-O. Mendoza-García, and J. de la Garza-Salazar, "High liposomal doxorubicin tumour tissue distribution, as determined by radiopharmaceutical labelling with <sup>99m</sup>Tc-LD, is associated with the response and survival of patients with unresectable pleural mesothelioma treated with a combination of liposomal doxorubicin and cisplatin," *Cancer Chemother. Pharmacol.*, vol. 74, no. 1, pp. 211-215, Jul. 2014, doi: 10.1007/s00280-014-2477-x.
- [10] W. W. Moses, "Fundamental limits of spatial resolution in PET," *Nucl. Instruments Methods Phys. Res. Sect. A Accel. Spectrometers, Detect. Assoc. Equip.*, vol. 648, pp. S236-S240, Aug. 2011, doi: 10.1016/j.nima.2010.11.092.
- [11] A. Rahmim and H. Zaidi, "PET versus SPECT: strengths, limitations and challenges," *Nucl. Med. Commun.*, vol. 29, no. 3, pp. 193-207, Mar. 2008, doi: 10.1097/MNM.0b013e3282f3a515.
- [12] M. M. Herth, V. L. Andersen, S. Lehel, J. Madsen, G. M. Knudsen, and J. L. Kristensen, "Development of a <sup>11</sup>C-labeled tetrazine for rapid tetrazine-trans-cyclooctene ligation," *Chem. Commun.*, vol. 49, no. 36, p. 3805, 2013, doi: 10.1039/c3cc41027g.
- [13] S. M. Ametamey, M. Honer, and P. A. Schubiger, "Molecular Imaging with PET," *Chem. Rev.*, vol. 108, no. 5,

pp. 1501-1516, May 2008, doi: 10.1021/cr0782426.

[14] C. Ash, M. Dubec, K. Donne, and T. Bashford, "Effect of wavelength and beam width on penetration in light-tissue interaction using computational methods," *Lasers Med. Sci.*, vol. 32, no. 8, pp. 1909-1918, Nov. 2017, doi: 10.1007/s10103-017-2317-4.

[15] R. E. Hendrick, "Spatial Resolution in Magnetic Resonance Imaging," in *Breast MRI*, New York, NY: Springer New York, 2008, pp. 31-45.

[16] E. Blumfield, D. W. Swenson, R. S. Iyer, and A. L. Stanescu, "Gadolinium-based contrast agents — review of recent literature on magnetic resonance imaging signal intensity changes and tissue deposits, with emphasis on pediatric patients," *Pediatr. Radiol.*, vol. 49, no. 4, pp. 448-457, Apr. 2019, doi: 10.1007/s00247-018-4304-8.

[17] R. A. Cloyd, S. A. Koren, and J. F. Abisambra, "Manganese-Enhanced Magnetic Resonance Imaging: Overview and Central Nervous System Applications With a Focus on Neurodegeneration," *Front. Aging Neurosci.*, vol. 10, Dec. 2018, doi: 10.3389/fnagi.2018.00403.

[18] Y.-D. Xiao, R. Paudel, J. Liu, C. Ma, Z.-S. Zhang, and S.-K. Zhou, "MRI contrast agents: Classification and application (Review)," *Int. J. Mol. Med.*, vol. 38, no. 5, pp. 1319-1326, Nov. 2016, doi: 10.3892/ijmm.2016.2744.

[19] F. Zoller, M. Eisenhut, U. Haberkorn, and W. Mier, "Endoradiotherapy in cancer treatment — Basic concepts and future trends," *Eur. J. Pharmacol.*, vol. 625, no. 1-3, pp. 55-62, Dec. 2009, doi: 10.1016/j.ejphar.2009.05.035.

[20] A. Morgenstern, F. Bruchertseifer, and C. Apostolidis, "Bismuth-213 and Actinium-225 – Generator

Performance and Evolving Therapeutic Applications of Two Generator-Derived Alpha-Emitting Radioisotopes," *Curr. Radiopharm.*, vol. 5, no. 3, pp. 221-227, Jun. 2012, doi: 10.2174/1874471011205030221.

[21] D. A. Scheinberg and M. R. McDevitt, "Actinium-225 in targeted alpha-particle therapeutic applications," *Curr. Radiopharm.*, vol. 4, no. 4, pp. 306-20, Oct. 2011, doi: 10.2174/1874471011104040306.

[22] S. Davies, B. J. Stenton, and G. J. L. Bernardes, "Bioorthogonal Decaging Reactions for Targeted Drug Activation," *Chim. Int. J. Chem.*, vol. 72, no. 11, pp. 771-776, Nov. 2018, doi: 10.2533/chimia.2018.771.

[23] X. Ji *et al.*, "Click and release: bioorthogonal approaches to 'on-demand' activation of prodrugs," *Chem. Soc. Rev.*, vol. 48, no. 4, pp. 1077-1094, 2019, doi: 10.1039/C8CS00395E.

[24] M. Czuban *et al.*, "Bio-Orthogonal Chemistry and Reloadable Biomaterial Enable Local Activation of Antibiotic Prodrugs and Enhance Treatments against *Staphylococcus aureus* Infections," *ACS Cent. Sci.*, vol. 4, no. 12, pp. 1624-1632, Dec. 2018, doi: 10.1021/acscentsci.8b00344.

[25] R. Rossin *et al.*, "Chemically triggered drug release from an antibody-drug conjugate leads to potent antitumour activity in mice," *Nat. Commun.*, vol. 9, no. 1, p. 1484, Dec. 2018, doi: 10.1038/s41467-018-03880-y.

[26] S. Hapuarachchige, Y. Kato, and D. Artemov, "Bioorthogonal two-component drug delivery in HER2(+) breast cancer mouse models," *Sci. Rep.*, vol. 6, no. 1, p. 24298, Jul. 2016, doi: 10.1038/srep24298.

[27] G. R. Ediriweera *et al.*, "Targeted and modular architectural polymers employing bioorthogonal chemistry

for quantitative therapeutic delivery,” *Chem. Sci.*, vol. 11, no. 12, pp. 3268-3280, 2020, doi: 10.1039/D0SC00078G.

[28] A. Forero *et al.*, “Phase 1 trial of a novel anti-CD20 fusion protein in pretargeted radioimmunotherapy for B-cell non-Hodgkin lymphoma,” *Blood*, vol. 104, no. 1, pp. 227-236, Jul. 2004, doi: 10.1182/blood-2003-09-3284.

[29] G. Paganelli *et al.*, “Pre-targeted locoregional radioimmunotherapy with 90Y-biotin in glioma patients: Phase I study and preliminary therapeutic results,” *Cancer Biother. Radiopharm.*, vol. 16, no. 3, pp. 227-235, Jul. 2001, doi: 10.1089/10849780152389410.

[30] S. J. Knox *et al.*, “Phase II trial of yttrium-90-DOTA-biotin pretargeted by NR-LU-10 antibody/streptavidin in patients with metastatic colon cancer,” *Clin. Cancer Res.*, vol. 6, no. 2, pp. 406-414, 2000.

[31] H. P. Kalofonos *et al.*, “Imaging of tumor in patients with indium-111-labeled biotin and streptavidin-conjugated antibodies: Preliminary communication,” *J. Nucl. Med.*, 1990.

[32] H. B. Breitz *et al.*, “Clinical optimization of pretargeted radioimmunotherapy with antibody-streptavidin conjugate and 90Y-DOTA-biotin,” *J. Nucl. Med.*, vol. 41, no. 1, pp. 131-140, 2000.

[33] A. Bates and C. A. Power, “David vs. Goliath: The Structure, Function, and Clinical Prospects of Antibody Fragments,” *Antibodies*, 2019, doi: 10.3390/antib8020028.

[34] S. M. Cheal *et al.*, “Curative multicycle radioimmunotherapy monitored by quantitative SPECT/CT-based theranostics, using bispecific antibody pretargeting strategy in colorectal cancer,” *J. Nucl. Med.*, vol.

58, no. 11, pp. 1735-1742, Nov. 2017, doi: 10.2967/jnumed.117.193250.

[35] S. M. Cheal *et al.*, “Theranostic pretargeted radioimmunotherapy of internalizing solid tumor antigens in human tumor xenografts in mice: Curative treatment of HER2-positive breast carcinoma,” *Theranostics*, vol. 8, no. 18, pp. 5106-5125, 2018, doi: 10.7150/thno.26585.

[36] K. D. Orcutt *et al.*, “Engineering an antibody with picomolar affinity to DOTA chelates of multiple radionuclides for pretargeted radioimmunotherapy and imaging,” *Nucl. Med. Biol.*, vol. 38, no. 2, pp. 223-233, 2011, doi: 10.1016/j.nucmedbio.2010.08.013.

[37] S. M. Cheal *et al.*, “Theranostic pretargeted radioimmunotherapy of colorectal cancer xenografts in mice using picomolar affinity 86Y- or 177Lu-DOTA-Bn binding scFv C825/GPA33 IgG bispecific immunoconjugates,” *Eur. J. Nucl. Med. Mol. Imaging*, vol. 43, no. 5, pp. 925-937, May 2016, doi: 10.1007/s00259-015-3254-8.

[38] S. M. Cheal *et al.*, “Alpha radioimmunotherapy using 225Ac-proteus-DOTA for solid tumors – Safety at curative doses,” *Theranostics*, vol. 10, no. 25, pp. 11359-11375, 2020, doi: 10.7150/thno.48810.

[39] F. C. J. van de Watering, M. Rijpkema, M. Robillard, W. J. G. Oyen, and O. C. Boerman, “Pretargeted Imaging and Radioimmunotherapy of Cancer Using Antibodies and Bioorthogonal Chemistry,” *Front. Med.*, vol. 1, Nov. 2014, doi: 10.3389/fmed.2014.00044.

[40] R. Schoffelen *et al.*, “Pretargeted immuno-positron emission tomography imaging of carcinoembryonic antigen-expressing tumors with a bispecific antibody and a68Ga- And18F-labeled hapten peptide in mice with human

tumor xenografts,” *Mol. Cancer Ther.*, vol. 9, no. 4, pp. 1019-1027, Apr. 2010, doi: 10.1158/1535-7163.MCT-09-0862.

[41] R. Schoffelen *et al.*, “Quantitative immuno-SPECT monitoring of pretargeted radioimmunotherapy with a bispecific antibody in an intraperitoneal nude mouse model of human colon cancer,” *J. Nucl. Med.*, vol. 53, no. 12, pp. 1926-1932, 2012, doi: 10.2967/jnumed.112.106278.

[42] S. Heskamp *et al.*, “ $\alpha$ -Versus  $\beta$ -Emitting radionuclides for pretargeted radioimmunotherapy of carcinoembryonic antigen-expressing human colon cancer xenografts,” *J. Nucl. Med.*, vol. 58, no. 6, pp. 926-933, Jun. 2017, doi: 10.2967/jnumed.116.187021.

[43] R. Schoffelen *et al.*, “Development of an imaging-guided CEA-pretargeted radionuclide treatment of advanced colorectal cancer: First clinical results,” *Br. J. Cancer*, vol. 109, no. 4, pp. 934-942, 2013, doi: 10.1038/bjc.2013.376.

[44] C. Bodet-Milin *et al.*, “Pharmacokinetics and dosimetry studies for optimization of pretargeted radioimmunotherapy in CEA-expressing advanced lung cancer patients,” *Front. Med.*, vol. 2, no. NOV, p. 27, Nov. 2015, doi: 10.3389/fmed.2015.00084.

[45] V. V. Demidov *et al.*, “Stability of peptide nucleic acids in human serum and cellular extracts,” *Biochem. Pharmacol.*, 1994, doi: 10.1016/0006-2952(94)90171-6.

[46] D. S. Youngblood, S. A. Hatlevig, J. N. Hassinger, P. L. Iversen, and H. M. Moulton, “Stability of cell-penetrating peptide-morpholino oligomer conjugates in human serum and in cells,” *Bioconjug. Chem.*, vol. 18, no. 1, pp. 50-60, Jan. 2007, doi: 10.1021/bc060138s.

[47] A. Vorobyeva *et al.*, “Development of an optimal imaging strategy for

selection of patients for affibody-based PNA-mediated radionuclide therapy,” *Sci. Rep.*, vol. 8, no. 1, p. 9643, Dec. 2018, doi: 10.1038/s41598-018-27886-0.

[48] A. Vorobyeva *et al.*, “Development of an optimal imaging strategy for selection of patients for affibody-based PNA-mediated radionuclide therapy,” *Sci. Rep.*, vol. 8, no. 1, p. 9643, Dec. 2018, doi: 10.1038/s41598-018-27886-0.

[49] B. L. Oliveira, Z. Guo, and G. J. L. Bernardes, “Inverse electron demand Diels–Alder reactions in chemical biology,” *Chem. Soc. Rev.*, vol. 46, no. 16, pp. 4895-4950, 2017, doi: 10.1039/C7CS00184C.

[50] P. E. Edem *et al.*, “Evaluation of the inverse electron demand Diels-Alder reaction in rats using a scandium-44-labelled tetrazine for pretargeted PET imaging,” *EJNMMI Res.*, vol. 9, no. 1, p. 49, Dec. 2019, doi: 10.1186/s13550-019-0520-y.

[51] E. J. L. Stéen *et al.*, “Trans-Cyclooctene-Functionalized PeptoBrushes with Improved Reaction Kinetics of the Tetrazine Ligation for Pretargeted Nuclear Imaging,” *ACS Nano*, vol. 14, no. 1, pp. 568-584, Jan. 2020, doi: 10.1021/acsnano.9b06905.

[52] A. Rondon *et al.*, “Pretargeted radioimmunotherapy and SPECT imaging of peritoneal carcinomatosis using bioorthogonal click chemistry: probe selection and first proof-of-concept,” *Theranostics*, vol. 9, no. 22, pp. 6706-6718, 2019, doi: 10.7150/thno.35461.

[53] O. Keinänen *et al.*, “Dual Radionuclide Theranostic Pretargeting,” *Mol. Pharm.*, vol. 16, no. 10, pp. 4416-4421, 2019, doi: 10.1021/acs.molpharmaceut.9b00746.

[54] O. Keinänen *et al.*, “Harnessing  $^{64}\text{Cu}/^{67}\text{Cu}$  for a theranostic approach to

- pretargeted radioimmunotherapy,” *Proc. Natl. Acad. Sci.*, p. 202009960, Oct. 2020, doi: 10.1073/pnas.2009960117.
- [55] S. Hapuarachchige, Y. Kato, and D. Artemov, “Bioorthogonal two-component drug delivery in HER2(+) breast cancer mouse models,” *Sci. Rep.*, vol. 6, no. 1, p. 24298, Jul. 2016, doi: 10.1038/srep24298.
- [56] S. Hapuarachchige *et al.*, “Cellular Delivery of Bioorthogonal Pretargeting Therapeutics in PSMA-Positive Prostate Cancer,” *Mol. Pharm.*, vol. 17, no. 1, pp. 98-108, Jan. 2020, doi: 10.1021/acs.molpharmaceut.9b00788.
- [57] R. Rossin *et al.*, “Chemically triggered drug release from an antibody-drug conjugate leads to potent antitumour activity in mice,” *Nat. Commun.*, vol. 9, no. 1, p. 1484, Dec. 2018, doi: 10.1038/s41467-018-03880-y.
- [58] G. R. Ediriweera *et al.*, “Targeted and modular architectural polymers employing bioorthogonal chemistry for quantitative therapeutic delivery,” *Chem. Sci.*, vol. 11, no. 12, pp. 3268-3280, 2020, doi: 10.1039/D0SC00078G.
- [59] I. Khan, P. F. Agris, M. V. Yigit, and M. Royzen, “In situ activation of a doxorubicin prodrug using imaging-capable nanoparticles,” *Chem. Commun.*, vol. 52, no. 36, pp. 6174-6177, 2016, doi: 10.1039/C6CC01024E.
- [60] B. L. Oliveira, Z. Guo, and G. J. L. Bernardes, “Inverse electron demand Diels–Alder reactions in chemical biology,” *Chem. Soc. Rev.*, vol. 46, no. 16, pp. 4895-4950, 2017, doi: 10.1039/C7CS00184C.
- [61] M. R. Eftink, M. L. Andy, K. Bystrom, H. D. Perlmutter, and D. S. Kristol, “Cyclodextrin inclusion complexes: studies of the variation in the size of alicyclic guests,” *J. Am. Chem. Soc.*, vol. 111, no. 17, pp. 6765-6772, Aug. 1989, doi: 10.1021/ja00199a041.
- [62] S. J. Spa *et al.*, “A Supramolecular Approach for Liver Radioembolization,” *Theranostics*, vol. 8, no. 9, pp. 2377-2386, 2018, doi: 10.7150/thno.23567.